Original Research Paper

Volume-8 | Issue-8 | August-2018 | PRINT ISSN No 2249-555X

Engineering

EFFECT OF HIGH-ENERGY MILLING AND SINTERING TEMPERATURE ON THE STRUCTURE OF A HARDMETAL

Adriano Corrêa Batista*	Thematic Network in Materials Engineering – REDEMAT, Federal University of Ouro Preto – UFOP, Ouro Preto, State of Minas Gerais, Brazil *Corresponding Author
Hellen Cristine Prata de Oliveira	Thematic Network in Materials Engineering – REDEMAT, Federal University of Ouro Preto – UFOP, Ouro Preto, State of Minas Gerais, Brazil
Macello Filgueira	Advanced Materials Laboratory – LAMAV, Northern Fluminense State University - UENF, Campos dos Goytacazes, State of Rio de Janeiro, Brazil
Maria Aparecida Pinto	Department of Metallurgy and Materials Engineering – DEMET, Federal University of Ouro Preto – UFOP, Ouro Preto, State of Minas Gerais, Brazil
Geraldo Lúcio Faria	Department of Metallurgy and Materials Engineering – DEMET, Federal University of Ouro Preto – UFOP, Ouro Preto, State of Minas Gerais, Brazil
Genivaldo Júlio Perpétuo	Department of Physics – DEFIS, Federal University of Ouro Preto – UFOP, Ouro Preto, State of Minas Gerais, Brazil

ABSTRACT This paper evaluated the effect of high-energy milling and sintering temperature on the structural characteristics of WC-10%Co. These samples were sintered at temperatures of 1350°C, 1400°C and 1450°C. The cooling rate of 100°C/h was used within the temperature range of 1000°C and 800°C to relieve residual stress from the sintering process. The samples were submitted to X-ray diffraction analysis with Rietveld refinement in order to characterize, at the atomic level, the effects of each processing stage on the material structure. The high-energy milling process may have accelerated the dissolution process of a large part of the WC particles during sintering, contributing to the formation of n phases. The characterization techniques were effective to evaluate the effects of high-energy milling, sintering temperature and residual stress on the structural characteristics of the composites investigated and the formation of amounts above 34% by weight of the Co_6W_6C and Co_3W_3C phases.

KEYWORDS : Conventional Sintering, Residual Stress, Rietveld Method, Phase Quantification.

INTRODUCTION

The composite formed by tungsten carbide (WC) and 10% by weight Cobalt (Co) stands out for its high hardness in the WC ceramic phase, and for the Co metal matrix that easily spreads and gives cohesion and toughness to the structure of the composite.

This material is largely used in industry because it offers an excellent combination of abrasion resistance, compressive strength, impact resistance, high elastic modulus, thermal shock and corrosion resistance. The mechanical and physical properties of hardmetals depend on the manufacturing process route, its microstructure and final composition [1-3]. Their main applications include cutting tools, drill bits for oil, water and gas wells, compaction matrices, high-energy milling components, among others [2,3].

Generally, the production of hardmetals consists of mixing dry powders (carbide and a binder metal) and/or milling, which may be of low or high energy. Milling is usually performed in an organic liquid medium with the addition of a lubricant, being paraffin the most used one. After milling, the liquid is removed by drying. Thereafter, the mixture follows the usual powder metallurgy route, being compacted, pre-sintered and finally sintered in an inert atmosphere or vacuum [4,5].

A very important variable in the sintering of compounds of the W-Co-C system is the concentration of carbon. The technical literature states that the reduction of the carbon content may cause decarburization of the WC, forming free W and C to react with the matrix phase (Co). This reaction results in phases, which, in the system in question, are predominantly Co_6W_6C and Co_2W_4C. It is noteworthy that due to the metastability of these phases, at 1000°C there may be Co_3W_3C formation. The formation of these phases deteriorates the good hardness/toughness ratio of the composite, making it very brittle [5-8].

In this context, this study investigated the effect of high-energy milling, sintering temperature and the cooling rate of the sintered parts. The strategy adopted consisted of using high-energy milling to obtain greater homogenization of the mixture and increase cohesion between WC particles and Co powder, prior to compaction and sintering. Afterwards, slow cooling was used in the region of 1000C to relieve the residual stress promoted by the sintering process, seeking a better relationship between hardness and fracture toughness. The results showed that high-energy milling and slow cooling at the rate of 100°C/h between 1000°C and 800°C used for residual stress relief benefits the formation of large amounts of metastable phases (Co_6W_6C and Co_3W_3C) in one of the most produced materials for metalworking cutting tools - WC-10% Co.

The aim of this study was to obtain information, at the atomic and structural levels, about the formation of phases in the processed hardmetals. Techniques such as X-ray diffraction (XRD, with the Rietveld Method), Scanning Electron Microscopy (SEM) and the Vickers microhardness test were employed.

So far, there have been only a few studies reporting this important issue, at most tackling it in a fragmented way, thus evincing a need for in-depth research using robust formalism.

MATERIALS AND METHODS

2.1. Materials

For the development of this study two powders were used, one of Co and another of WC with average particle sizes of 3.6µm and 125nm, respectively. The chemical compositions of these materials are displayed in Tab. 1.

Table 1 – Chemical compositions of Co and WC powders (wt.%).

Co powder											
O_2	C	S	Ni	Fe	Cu	Zn	Mn	Na	Mg	Ca	Co
0.55	1500	30	500	<10	<20	<20	<10	<10	<10	<10	Base
%	ppm	ppm	ppm	ppm	ppm	ppm	ppm	ppm	ppm	ppm	
WC powder											

C_{Total}	C_{free}	O	Al	Ca	Cr	Fe	Mo	Ni	Si	Sn	W
6.18	0.14	0.10	2	2	10	35	12	4	<5	<2	Base
%	%	%	ppm	ppm	ppm	ppm	ppm	ppm	ppm	ppm	

Characterization of WC and Co powders

WC and Co powders were subjected to X-ray diffraction characterization. This first stage intended to identify phases of WC and Co powders. The Rietveld Method was used to quantify the phases and obtain information about the structures of each phase with respect to lattice parameters, atomic positions, density, unit-cell volume, and refinement quality indices. The equipment used and the conditions of measurement were the same as those used in the characterization of the composite, as described later.

Processing of the composite

WC powder was mixed with 10wt.% Co powder for 40 minutes in a high-energy ball mill, model SPEX 8000. The ball-to-powder mass ratio was 3:1, until approximately 25% of the 51cm^3 internal-volume ...vessel was filled [9-11].

Subsequently, compaction of the mixed powders forming the composite was performed in a cylindrical matrix under a uniaxial pressure of 300MPa (manufacturing of the green compact). After that, a vacuum tubular resistance furnace with a constant pressure of 10^{-2}mbar was used. Three groups of samples with the same composition (WC-10% Co) were sintered, but at different sintering temperatures of 1350°C, 1400°C and 1450°C, for 60 minutes [4,12]. The cooling rate of 100°C/h within the temperature range of 1000°C - 800°C was used to relieve residual stress from the sintering process, seeking a better relationship between hardness and fracture toughness. Cooling was also slowed down below the temperature of 800°C, allowing the phase transition from Co (fcc) to (hc) to seek a better relationship between mechanical properties.

Characterization of the composite

The densities of the sintered samples were measured using the Archimedes' principle [13,14]. Afterwards, microstructural analyses were performed using Scanning Electron Microscopy/Energy Dispersive Spectroscopy (SEM-EDS) to evaluate the effect of the processing on the WC particles' morphology, on the interaction of such particles with the Co metal matrix, and on pore size observation. In addition to those variables, potential formation of metastable phases such as phases was also described. The images were generated with a secondary electron detector.

Pore volume fraction was calculated by the quantitative metallography method [15,16]. Micrographs were converted into binary images with threshold adjustment so that the pores would highlight the black contrast in relation to other areas of the images. The software used was Leica Application Suite version 4.6, which was calibrated to recognize all spots with identical color and contrast as pores. Then, the software calculated the area of the recognized spots and divided it by the total area of the image. The obtained fraction is considered the fraction of pores measured by the area method.

Following the recommendations of ASTM international standard E384, the Vickers microhardness test was performed to evaluate the material's resistance to localized plastic deformation [17,12]. A load of 200gf for 10s was used.

The fracture toughness of the material was measured with the Palmqvist method. Fracture toughness is given by

$$K_{IC} = 0.0889\sqrt{\frac{HVxF}{L_i}}$$

where $L_i = a_1+a_2+a_3+a_4$ is the sum of the lengths of the corner cracks, F is the indentation load in Newton, and HV is the Vickers hardness value in N/m2 [14].

For the structural and quantitative characterization of the phases in the sintered structure, the X-ray diffraction technique was used. The quantification of the phases by means of X-ray diffraction assumes that the sum of integrated relative intensities of the crystalline phases' reflections is proportional to the amount of diffractive unit cells. Therefore, this technique provides the diffracted fraction of the material's component phases at the atomic level [18]. For the quantification of the phases with this technique, the use of a standard reference material is necessary, so that its crystallographic behavior and its quantity by weight can be known. It is called internal standard material because it is mixed with the material whose phases will be quantified, when still in the powder form. This way, a calibration curve is created, which, for sintered parts, is impracticable. In this context, this technique ends up being little used in the field of powder metallurgy for sintered parts [18].

However, X-ray diffraction data allow determining crystallographic parameters and quantification of all phases using the external standard method incorporated into Rietveld refinement routines [18,19].

In view of the various advantages over traditional internal-standard-based techniques, in this study the Rietveld method was used for that purpose. It should be noted that this method has been used for systems of gradually increasing complexity, either in terms of number of phases or degree of structure order [18,20]. These applications have demonstrated that the Rietveld method can provide very precise values of the relative and/or absolute amounts of various materials' component phases [18,20].

The phases of the sintered samples were identified using a Shimadzu XRD 7000 X-ray diffractometer with Cu K radiation, operated at 40kV voltage and 30mA current, in addition to a graphite monochromator. Interval 2 ranged from 5° to 125° with a step of 0.01°, and a time of 3s per step. Room temperature was kept constant at 18°C throughout the data acquisition process [18]. The obtained diffractograms were compared with files from the Inorganic Crystal Structure Database (ICSD)/CrystMet [21]. For the quantitative analysis of the phases with the Rietveld method, the General Structure Analysis System - GSAS software was used [19,22,23].

The diffraction patterns of the samples were submitted to a Rietveld analysis, as provided in the GSAS software package [19,24]. The Pseudo-Voigt/4 function with asymmetry correction was used for the quantitative phase analysis [24,25]. The general refinement parameters were: phase scale factors, background radiation coefficients (Shifted Chebyschev), unit cell parameters, zero displacement error, peak form parameters, and preferential orientation coefficients. When necessary, the March-Dollase ellipsoidal preferred orientation correction algorithm was used [23,25-27].

RESULTS AND DISCUSSION

3.1. Characterization of WC and Co powders

Tab. 2 shows the lattice parameters and refinement indices for the WC powder measured by the X-ray diffraction technique and the Rietveld method. Fig. 1 shows a comparison between the X-ray diffractogram (yobs) experimentally obtained and the one calculated with the Rietveld (ycal) refinement. The data analysis indicated that the WC powder used is a high-purity metal powder, as the WC phase was the only one identified by the technique. The χ^2 value was equal to 1.66%, indicating a small difference between the measured and the calculated data, which reflects the quality of the method used for characterizing the WC-powder atomic structure.

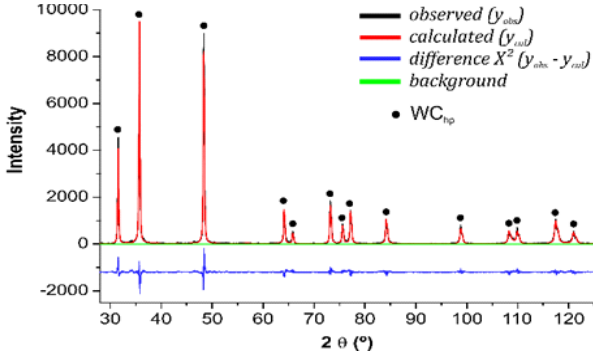

Figure 1 – WC-powder X-ray diffraction data refinement (Refinement quality indices: Rwp 13.43%, Re 8.09%, χ^2 1.66% and R_B 2.73%).

Table 2 – Lattice parameters, amount in each phase, volume and density of the unit cell in the WC, Co and mixture of WC-10%Co powders.

Powders	a (Å)	b (Å)	c (Å)	Volume (Å^3)	Density (g/cm3)	Phase (%)	Crystallography
WC	2.9051	2.9051	2.8387	20.748	16.523	100.00	WC/P6 $\bar{m}$2 (187) hp
Co	2.5082	2.5082	4.0742	22.197	8.819	75.60	Co/P63/mmc (194) hc
	3.5445	3.5445	3.5445	44.531	8.790	24.40	Co/Fm3 $\bar{m}$ (225) fcc
Mixture WC-10%Co	2.9056	2.9056	2.8393	20.710	20.360	90.51	WC/P6 $\bar{m}$2 (187) hp
	2.5458	2.5458	4.1464	23.270	10.010	9.49	Co/P63/mmc (194) hc

The Co powder diffractogram in Fig. 2 shows noisy background and broad peaks, indicating the presence of an amorphous fraction. After the Inorganic Crystal Structure Database (ICSD) analysis, two phases were observed: a face-centered cubic (fcc) and a hexagonal compact *(hc)* phase [18,21]. The peak at position 51.56° appears only in the Co *(fcc)* structure formed above 427°C and retained in its structure due to the rapid cooling in the production process. The other peaks with intensity below 84cps represent the beginning of the formation stage and/or crystallinity increase of the compact hexagonal phase, promoted by the powder production process through water atomizing. Tab. 2 displays the lattice parameters, density and fractions of the fcc and hc Co phases measured by Rietveld refinement of the experimental data.

Characterization of the high-energy milling product of mixture 90% WC and 10% Co

In the second stage, powders were mixed by high-energy milling in the proportions of 90% WC and 10% Co by weight. In this process, particles are repeatedly crushed, cold-welded, fractured and welded again. This way, Co was distributed throughout the mixture composition, and adequate homogeneity was obtained.

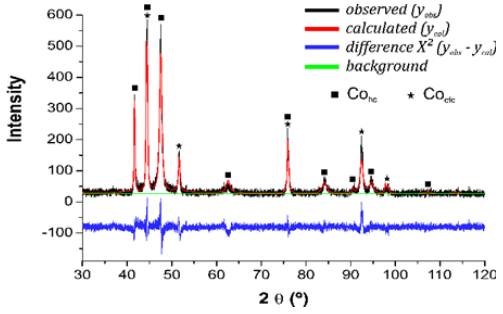

Figure 2 – Co-powder X-ray diffraction data refinement (Refinement quality indices: R_{wp} 18.81%, Re 15.80%, χ^2 1.19% and R_B 1.69%).

The influence of milling on the composition of the phases at the end of this procedure was evaluated using the X-ray diffraction and the Rietveld methods. Tab. 2 shows the composition of the phases in the WC-10%Co composite sample and other information obtained with X-ray diffraction pattern refinement. Fig. 4 displays the diffractogram of the mixture of powders forming the WC-10%Co composite, which presents low-noise background with well-defined WC *(hp)* and Co *(hc)* phases, with little-broad peaks and considerable intensities.

After the Inorganic Crystal Structure Database (ICSD) analysis, peak overlaps were observed for WC and Co in the range of 46º to 85º, undergoing a slight enlargement [18,21]. The other peaks are in agreement with the crystallographic databases, indicating the presence of the WC (*hp*) phase (90.51%) together with the Co (hc) phase (9.49%). The Co (*fcc*) phase was not accepted by the refinement, generating strong divergences and making it impossible to confirm the presence of Co (*fcc*).

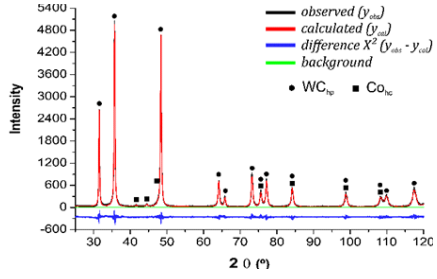

Figure 3 – X-ray diffraction data refinement of the mixture of WC and Co powders (Refinement quality indices: R_{wp} 12.27%, R_e 9.73%, 1.26% and RB 3.94%).

Tab. 2 exhibits the lattice parameters and the volume and density values of the unit cell of the powdered WC phase and the WC phase after mixing, obtained with X-ray diffraction data refinement. An increase can be observed in the unit cell density of the WC present in the mixture, rising from 16.53g/cm^3 to 20.36g/cm^3.

There was no significant variation in the dimensions of lattice parameters a, b and c or in the unit-cell volume, as can be seen in Tab. 2. By analyzing these data and calculating the total atomic mass value of the WC powder unit cell (hp), it was observed that a structural density variation without a significant lattice parameter variation could only be explained by considering the change in the structure's number of atoms as a result of high-energy milling. It was found that the calculated structural density value converges to the measured value, when considering the existence of one Co atom per WC unit cell. Also, high-energy milling causes deformations in the crystalline lattice and grain contours created during the process, promoting a high diffusion rate and also allowing that kinetic reactions occur between WC and Co [10,11]. Owing to the Co atomic radius, it is physically possible to incorporate it into the interstices of the WC lattice, increasing the density and maintaining the positions of the W and C atoms. Therefore, the lattice parameters (a, b and c) and volume values may have low fluctuations with a good approximation to the atomic packing factor value for this model (hp). In this sense, it is hypothesized that during high-energy milling some Co atoms were mechanically introduced into the interstices of the WC unit cells.

Another important observation that can be made by analyzing Tab. 2 is that the existing Co fraction was initially fcc and after high-energy milling it was almost entirely transformed into an hc structure. It is assumed that, during high-energy milling, the Co (fcc) phase underwent an intense plastic deformation, which, given the low stacking fault energy of Co, was accommodated in the form of a possible martensitic transformation, that is, a transformation of structure fcc into hc, induced by plasticity [28-30].

Characterization of the sintered composite Microstructure and chemical analysis

Samples of the mixture from the high-energy milling process were subjected to different sintering temperatures. The products of this step were characterized by SEM to evaluate pore fraction, along with EDS analysis to chemically characterize microstructures.

In the WC-10%Co composite sintered at 1350°C (Fig. 4-a and Tab. 3), an agglomeration of WC particles (light gray region) dispersed through the Co matrix (dark gray region) was observed [31]. The porosity of the hardmetal at this temperature has a wide size distribution with relatively rounded morphologies. Although Spot 1 presents dark gray color typical of regions with high Co concentration, the EDS spot chemical analysis allows assuming that WC grains are covered by a Co thin film. Spot 2 shows a light gray region, where the amount of W indicates WC grain formation. Spots 3, 4 and 5 show dark gray regions with amounts of Co and W nearby, indicating a possible stoichiometry of the Co_6W_6C and Co_3W_3C phases.

Fig. 4-b shows the composite sintered at 1400°C, where the amount of WC agglomerates (lighter-colored region) decreased, with rounded morphology dispersed through the Co matrix, indicating dissolution of WC agglomerates by Co. At this temperature, the smallest pores were closed as a result of the sintering process, leaving only the largest pores, but already in the initial process of closure, with a quite rounded morphology.

The data in Tab. 3 show spots in several regions of the sample where the three chemical elements of the composite appear together, making it difficult to identify WC grains, always embedded with Co, and Co pools impregnated with W and C [31].

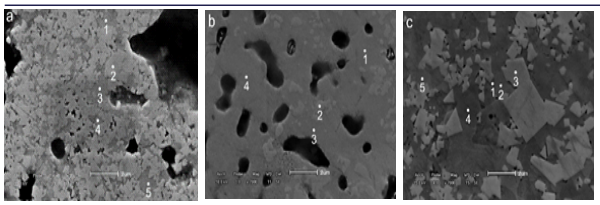

Figure 4 – Micrographs of WC-10%Co composite submitted to high-energy milling and sintering at temperatures (a) 1350°C; (b) 1400°C; (c) 1450°C.

Spot 1, in the dark gray region with high Co concentration, indicates the presence of WC grains covered by a Co thin film. Spot 2 shows a light gray region with very high amounts of W and C, indicating the WC-grain-forming region. Spots 3 and 4 show dark gray regions with amounts of Co and W nearby, indicating a possible stoichiometry of the Co_6W_6C and Co_3W3_C phasses.

In Fig. 4-c, the composite sintered at 1450°C shows the stage where the WC particles regrouped giving continuity in grain growth, whose morphology differs from that of the other samples. The presence of small rounded pores dispersed throughout the sample is also observed, indicating the effectiveness of the sintering. It is worth noting that in W-Co-C systems the eutectic melting temperature of Co is 1275°C, so at 1350°C the matrix is already liquid and W experiences a temperature range where its solubility in Co is significant [6,32]. Tab. 3 shows the EDS results, which confirm the presence of regions with high W concentrations, and regions with the presence of Co always accompanied by proportional quantities of W. The spot values indicated in Tab. 3 show some chemical stability with well-defined regions of WC (3) grains and the Co (1, 2, 4 and 5) matrix with strong evidence of metastable phase formation [6,32].

Table 3 – Semiquantitative chemical analysis by EDS of the sample sintered at 1350ºC, 1400ºC and 1450ºC, for spots 1 through 5 (at.%), as indicated in Fig. 4 (a,b,c).

Temperature	Element	Spot 1	Spot 2	Spot 3	Spot 4	Spot 5
1350ºC	C	64.46	60.31	57.01	56.55	47.88
	Co	9.70	12.18	17.99	19.07	24.72
	W	25.83	27.49	24.98	24.37	27.39
1400ºC	C	49.53	75.85	40.76	47.17	---
	Co	18.82	2.92	26.69	20.48	---
	W	31.64	21.22	32.53	32.34	---
1450ºC	C	58.20	53.01	70.51	45.26	44.18
	Co	14.07	14.07	---	16.26	16.80
	W	11.83	15.11	29.48	16.44	22.21

Diffraction X-ray and Rietveld analyses

The use of XRD in the samples sintered at 1350°C, 1400°C and 1450°C identified the WC (*hp*) phases of space group $P\bar{6}m2$ (187), the Co (*hc*) phases of space group P63/mmc (194), Co_6W_6C (*fcc*) of space group $Fd\bar{3}m$ (227) and Co_3W_3C *(fcc)* from space group $Fd\bar{3}m$ (227) [33,34]. Figures 5, 6 and 7 display the Rietveld graphs, the refinement quality indices, with y_{cal} modeling y_{obs} and the χ^2 value representing the difference between them.

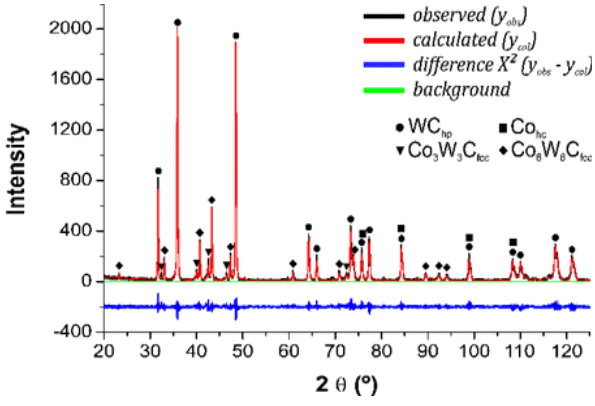

Figure 5 – Sample sintered at 1350°C (Refinement quality indices: Rwp 17.80%, Re 12.04%, χ^2 1.49% and R_B 8.93%).

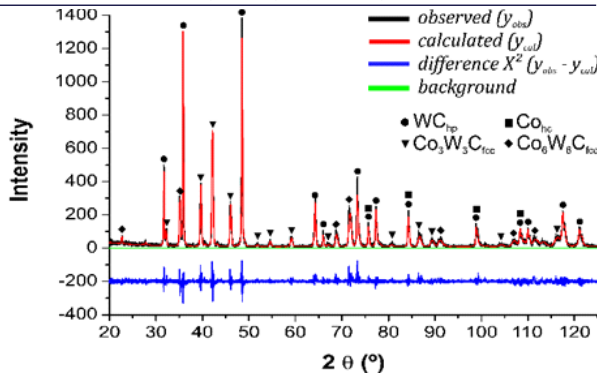

Figure 6 – Sample sintered at 1400°C (Refinement quality indices: Rwp 19.25%, Re 14.14%, χ^2 1.65% and R_B 9.713%).

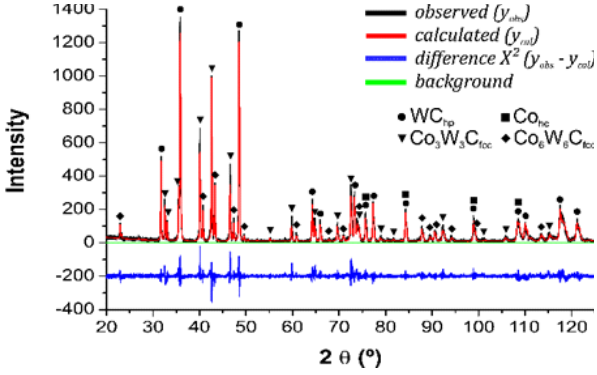

Figure 7 – Sample sintered at 1450°C (Refinement quality indices: Rwp 20.53%, Re 14.84%, χ^2 1.84% and R_B 11.91%).

With the information obtained from the X-ray diffraction data refinement by the Rietveld method, presented in Tab. 4, transformations were observed in the microstructures by quantification of the present phases, revealing a constant production of metastable phases with the increase of the sintering temperature.

Table 4 – Quantification of phases obtained with the Rietveld method for samples sintered at 1350°C, 1400°C and 1450°C.

Sintering Temperature		1350°C	1400°C	1450°C
Phases present (%)	WC (hp)	63.619	52.456	40.212
	Co_6 W_6 C (cfc)	24.820	1.188	14.330
	Co_3 W_3 C (cfc)	9.312	46.053	45.340
	Co (hc)	2.240	0.303	0.104

Tab. 4 indicates the low occurrence of the Co (hc) phase in the sample sintered at 1400°C and 1450°C, which, despite its small quantity (0.303% and 0.104%), as identified by the refinement, the presence of this phase in the refinement routine was crucial. Without it, divergences would occur and the refinement would be interrupted. Carbon and tungsten have high solubility in cobalt, being tungsten more soluble [6,7,32,35].

Besides the quantification of the phases, the Rietveld method provided values for lattice parameters, unit-cell volume and density (Tab. 5 and 6) [33,34]. With this information, the relationship between lattice parameters, unit-cell volume and density was observed, showing, at the atomic level, the effects of the sintering process on the WC and Co structures, taking into account all the production process variables relevant to this system.

Dissolution of the WC phase by Co reached 26.38% at 1350°C, 37.54% at 1400°C, and 49.79% at 1450°C, as can be seen in Tab. 4.

Table 5 – Information about the lattice parameters obtained by the Rietveld method for the sintered samples.

Parameters	Phase	1350°C	1400°C	1450°C
a(Å)	WC (hp)	2.9051	2.9043	2.9045
	Co_6W_6C (fcc)	10.8994	10.9710	10.8885
	Co_3W_3C (fcc)	11.0690	11.1949	11.0506
	Co (hc)	2.5000	2.5061	2.5000

b(Å)	WC (hp)	2.9051	2.9043	2.9045
	Co_6W_6C (fcc)	10.8994	10.9710	10.8885
	Co_3W_3 C (fcc)	11.0690	11.1949	11.0506
	Co (hc)	2.5000	2.5061	2.5000
c(Å)	WC (hp)	2.8361	2.83562	2.8360
	Co_6W_6 C (fcc)	10.8994	10.9710	10.8885
	Co_3W_3 C (fcc)	11.0690	11.1949	11.0506
	Co (hc)	4.0920	4.0303	4.0920

The Co_6W_6C phase is formed as a result of the WC-Co reaction that is promoted by numerous high-speed diffusion paths, such as distortions in the crystalline lattices and grain boundaries created during the milling process, which allows a high diffusion rate therefore allowing reactions between WC-Co to happen kinetically [11,30].

Table 6 – Information about volume and density obtained by the Rietveld method for the sintered samples.

	Phase	1350°C	1400°C	1450°C
Volume ($Å^3$)	WC (hp)	20.730	20.714	20.720
	Co_6W_6C (fcc)	1294.810	1320.600	1290.940
	Co_6W_6 C (fcc)	1356.200	1403.047	1349.480
	Co (hc)	22.160	21.923	21.548
Density (g/cm^3)	WC (hp)	22.860	20.745	21.785
	Co_6W_6 C (fcc)	15.491	10.390	15.331
	Co_6W_6C (fcc)	14.689	15.156	15.542
	Co (hc)	8.201	8.611	8.837

During the sintering process, the WC phase dissolution together with the large depletion of C led to the formation of the Co_6W_6C phase, which at 1350°C contributed 24.82% of the phases in the sintered sample, followed by the Co_3W_3C phase with 9.31%. This dynamic of metastable phase formation evolved as the sintering temperature increased, which is when the Co_6W_6C phase transformation occurs, producing large amounts of the Co_3W_3C phase at 1400°C [5-7]. At 1450°C, the Co_3W_3C phase stabilized and the Co_6W_6C phase was formed again. Such phase transformation can be observed by the lattice parameters oscillation of the phases, as shown in Tab. 5 and 6. At 1400°C, the Co_6W_6C phase had its highest values for lattice parameter a and volume, with the smallest density, indicating fluctuation of the cohesive energy of the unit cell undergoing the rearrangement thereof for the Co_3W_3C phase. This may be related to a continuous depletion of carbon due to the presence of oxygen adsorbed by the powder particles during the production process, compaction and some amount of oxygen retained in the indoor wall of the tube furnace [8].

By comparing the values for lattice parameters and unit-cell volume (Tab. 5 and 6) at the three sintering temperatures, it was noted that the WC phase presented the highest values for lattice parameters and volume at 1350°C and 1450°C, indicating differentiated dynamics in the dissolution and formation of metastable phases, here divided into three stages.

In the first stage at 1350°C, the sintered sample had the highest unit-cell density of the WC phase, indicating that the dissolution process did not reach its dynamic peak. Co diffuses slowly, reflecting the lowest production of metastable phases allied to its higher volume, fluctuation of lattice parameter c of the unit cell and the lowest density measured for that phase. These factors promote instability in the atomic arrangement of these phases when submitted to the sintering temperatures adopted here (Tab. 5 and 6).

In the second stage, at 1400°C the WC phase presented the lowest values for lattice parameters, volume, density (Tab. 3, 5 and 6). At this temperature, therefore, the WC phase showed some stability in its structure. Co continued to interact strongly with W and C, promoting intense formation and transformation from Co_6W_6C to Co_3W_3C phases with greater intensity [7,35].

In the third stage at 1450°C, WC regrouped, thus promoting grain growth; at that point the process of diffusion decreased. This can be observed by the increased WC unit-cell density and the atomic rearrangement between the metastable phases due to fluctuation of the values of its lattice parameters, unit-cell volume and almost total dissolution of the Co phase (Tab. 5 and 6).

Density and Vickers hardness / fracture toughness

In terms of sintering effectiveness, it was observed that temperatures 1350°C and 1400°C were not sufficient to consolidate the sintering structure. This can be noticed by the presence of large pores randomly dispersed through the sample. At 1450°C, the sintered structure reached almost full consolidation, with small pores of rounded morphology dispersed through the sample.

In order to evaluate sintering effectiveness, the Archimedes' density and total porosity of the samples sintered at the three temperatures were measured (Tab. 7).

It was clearly observed that the density increased as the sintering temperature increased, owing to the evolution of particle agglomeration and matter transport, thus closing the pores.

It can be observed that the Archimedes' density values evolve as a function of temperature, coming close to the theoretical density predicted for this composite at the highest sintering temperature [30,36-38].

Table 7 – Physical properties of the sintered samples, Archimedes' density (D) and porosity (P).

Sintering Temperature	D (g/cm^3)	S.D.(g/cm^3)	P (%)	S.D.(%)
1350C	12.08	0.75	20.10	2.45
1400C	13.13	0.83	14.23	0.83
1450C	14.59	0.10	0.31	0.20

Note: The theoretical density obtained by the Rule of Mixtures is equal to 14.6 g/cm^3. S.D. stands for Standard Deviation and P represents the pore volume fraction measured by quantitative metallography.

The microhardness and fracture toughness values of the sintered samples were calculated, and the results are shown in Table 8. It was noted that with an increase in the sintering temperature there was also an increase in hardness and fracture toughness. At the sintering temperature of 1350°C (Fig. 4-a), the structure of the sintered samples showed 20% porosity. This was the beginning of the WC particle consolidation associated with metastable phase formation indicated by SEM/EDS and phase quantification by the Rietveld method (Tab. 3 and 4) [7].

Table 8 – Average of the Vickers microhardness and fracture toughness values of the sintered samples.

Sintering Temperature (°C)	HV 200gf/10s (GPa)	Standard Deviation (GPa)	K_{IC} Fracture toughness ($MPa.m^{1/2}$)	Standard Deviation ($MPa.m^{1/2}$)
1350	12.5	0.8	7.79	0.3
1400	15.4	1.6	9.16	0.2
1450	16.7	0.9	8.91	0.4

At 1400°C (Fig. 4-b), the porosity decreased, reaching 14%, which triggered an intense dissolution of the WC particles and the transition from the Co_6W_6C phase to the Co_3W_3C phase (Tab. 3 and 4), thus increasing the composite's hardness and fracture toughness [7,30,37-39]. At temperature 1450°C (Fig. 4-c), porosity decreased drastically, reaching 0.3%, where the composite reached its maximum densification. This temperature enabled the formation of a large part of the Co_3W_3C phase (Tab. 3 and 4), which, together with the atomic regrouping and the WC grain growth, reached the highest hardness value for this composite in this study [7,8,40,41].

Relief of residual stress

The Sintering Conditions graph (Fig. 8) shows the cooling temperature range between 1000°C and 800°C set at the rate of 100°C/h where the residual stress relief was performed. The range 1000°C - 800°C is the temperature indicated for the beginning of the phase formation. The cooling process reduced the temperature of the sintering stages 1350°C, 1400°C and 1450°C) to 1000°C in 15 minutes.

This relatively rapid cooling produces intense residual stress throughout the microstructure of the material. Such residual stress produces strong distortions in the unit cells of the present phases, inhibiting the atomic organization and possible phase transitions. The relief of this residual stress allowed atomic reorganization, eliminating distortions in the lattice and completing the phase transitions.

The thermal treatment of the samples in this temperature range was carried out for 2h, which kept active the dissolution of the WC phase and the formation of the Co_6W_6C and Co_3W_3C phases. This heat

treatment also caused the disappearance of possible amorphous regions ($Co_3W_{10}C_{3.4}$) and the W_2C phase [8,42,44].. However, it is worth mentioning that the heat treatment may result in a decrease both in the carbon and oxygen contents due to the internal reduction processes.

According to the W-C phase diagram, W_2C is thermodynamically unstable. Below 1250°C, it can decompose into WC and W during cooling of the WC-Co particle. This decomposition can also result from the heat treatment at 920°C. The heat treatment where Co is present forms the phases as mentioned above, and Co can be totally consumed by these reactions. [45].

In the final phase, between temperatures 800°C and 25°C, cooling was kept slow thus promoting the martensitic transformation of the *fcc* phase from Co to hc. It is known that pure cobalt has the stable *hc* phase below the temperature of 417°C and, above that, it undergoes a martensitic transformation and starts to present the cfc phase. This transformation is slow, and a metastable *fcc* phase can be retained during a rapid cooling process. The *fcc* phase presents better ductility and work-hardening strengthening than that of the hcp phase. As can be seen in Fig. 8, in this study we used 3h for the cooling, seeking to benefit the martensitic transformation of the cfc phase into the hcp phase of cobalt [28,46].

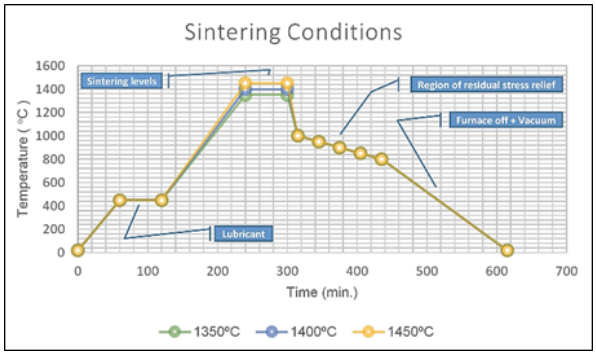

Figure 8 – Sintering conditions with a time of 1 hour for the sintering stages at 1350ºC, 1400ºC and 1450ºC and residual stress relief in the range from 1000C to 800C for 2 hours.

Finally, the factors that contributed to the high amount of phases were the nanometric particle size of the WC powder, which allowed greater interaction of its particles with those of Co, associated with high-energy milling, diffusing the cobalt atoms in the hp structure of the WC powder. Additionally, the amount of oxygen retained in the Co (0.55wt.%) and WC (0.10wt.%) powder structures, together with the oxygen incorporated and retained during compaction of the powders to produce the samples, differed during sintering, which resulted in a large depletion of C, indicating the most favorable condition for the production of η phases – Co_6W_6C and Co_3W_3C[8].

Due to the carbon deficiency and the heat treatment, a high phase formation took place, which weakened the plasticity of the binder phase, leading to deterioration of the mechanical properties of the samples increasing their hardness and reducing their fracture toughness [47]. The slow cooling process after the heat treatment promoted the martensitic transformation of the cfc phase of Co into hcp, interfering with the value of hardness and fracture toughness given that the hcp phase decreased its hardness.

CONCLUSIONS

The following conclusions can be drawn from the present study. The characterization techniques employed here, mainly X-ray diffraction and the Rietveld method, proved efficient to evaluate the effect of high-energy milling, sintering temperature and residual stress relief on the structural characteristics of the composites investigated. The external standard method associated with the use of CIF - Crystallographic Information File, obtained by calculation of *Ab Initio*, potentiated and enabled the use of the Rietveld method for the analysis of the sintered materials.

The effects of high-energy milling on the mixture of WC and Co powders were observed by comparing the XRD data refinement of WC powder, Co powder, and the mixture of WC and Co powders. It was shown that high-energy milling forced the Co atoms to occupy the interstices of the hp unit cells of the WC powder. This effect can be noted in the unit-cell density value of the WC powder after milling with Co powder. This event may have accelerated the dissolution process of a large part of the WC particles during sintering, contributing to the large formation of Co_6W_6C and Co_3W_3C phases.

Other factors that contributed to all the transformations occurring in the composite include the nanometer particle size of the WC powder, which allowed for greater interaction of its particles with those of Co, in addition to the amount of oxygen retained in Co (0.55% by weight) and WC (0.10% by weight). This, in addition to the oxygen incorporated and retained in the samples in the compaction of the powders, transferred the C atoms out of the samples during the sintering process, resulting in a large depletion of C, indicating the most favorable condition for the formation of η phases – Co_6W_6C and Co_3W_3C.

During the sintering process, (Archimedes') density increased as the sintering temperature increased, being near the theoretical density at temperature 1450°C. The WC phase dissolution together with C reduction triggered the formation of the Co_6W_6C phases, which at 1350°C contributed 24.82% of the phases in the sintered sample, followed by the Co_3W_3C phase with 9.31%. At 1400°C, the Co_6W_6C phase had its highest values for lattice parameter and volume, with the smallest density, indicating cohesive energy fluctuation of the unit cell undergoing a rearrangement thereof for the Co_3W_3C phase. At 1450°C, the Co_3W_3C phase stabilized and the Co_6W_6C phase was formed again.

The increase in (Archimedes') density and the formation of the Co_6W_6C and Co_3W_3C metastable phases in the composite led to a significant increase in the hardness of the material. While at 1350°C the density was 12.08g/cm^3 and the total fraction of metastable phases was 34.1%, at 1450°C density was 14.59g/cm^3 and the total fraction of metastable phases was 59.6%. The hardness of the sintered samples at each of such temperatures were, respectively, 12.5GPa and 16.7GPa. Fracture toughness was also measured, and values between 7.79MPa.m$^{1/2}$ and 9.16MPa.m$^{1/2}$ were found – indicative of a hard and fragile material.

Carbon deficiency and residual stress relief contributed to the high η phase formation observed, which weakened the plasticity of the binder phase, leading to deterioration of the mechanical properties of the samples, making the material hard and fragile. The slow cooling process after the heat treatment promoted the martensitic transformation of the cfc phase of Co into hcp, interfering with the value of hardness and fracture toughness.

ACKNOWLEDGEMENT

This study was financially supported by the Coordination for the Improvement of Higher Education Personnel (CAPES Foundation), Brasília, DF, Brazil; and the Federal University of Ouro Preto (UFOP), Ouro Preto, MG, Brazil.

REFERENCES

[1] Ortner HM, Ettmayer P, Kolaska H, Smid I. The history of the technological progress of hardmetals. International Journal of Refractory Metals and Hard Materials. 2015; 49; 3-8.
[2] Konyashin I, Ries B, Hlawatschek S, Mazilkin A. Novel industrial hardmetals for mining, construction and wear applications. International Journal of Refractory Metals and Hard Materials. 2018; 71; 357-365.
[3] Grilli ML, Bellezze T, Gamsjäger E, Rinaldi A, Novak A, Balos S, et al. Solutions for Critical Raw Materials under Extreme Conditions. A Review by Materials. 2017; 10(3); 285.
[4] Allibert CH. Sintering features of cemented carbides WC–Co processed from fine powders. International Journal of Refractory Metals and Hard Materials. 2001; 19; 53-61.
[5] Pollock CB, Stadelmaier HH. The eta carbides in the Fe–W–C and Co–W–C systems. Metallurgical and Materials Transactions B. 1970; 1; 767.
[6] Fernandes CM, Senos AMR. Cemented carbides phase diagrams: A review. International Journal of Refractory Metals and Hard Materials. 2011; 29; 405-418.
[7] Lavergne OA, Robaut FB, Hodaj FA, Allibert CH. Mechanism of Solid-State Dissolution of WC in Co-Based Solutions. Acta Materialia. 2002; 50; 1683-1692.
[8] Yang Q, Yang J, Yang H, Ni G, Ruan J. Synthesis of ultrafine WC-10Co composite powders with carbon boat added and densification by sinter-HIP. International Journal of Refractory Metals and Hard Materials. 2017; 62; 104-109.
[9] Zhang FL, Wang CY, Zhu M. Nanostructured WC/Co composite Powder Prepared By high energy Ball Milling. Scripta Materialia. 2004; 49; 1123-1128.
[10] Kim J, Kang S. WC platelet formation via high-energy ball mill. International Journal of Refractory Metals and Hard Materials. 2014; 47; 108-112.
[11] Enayati MH, Aryanpour GR, Ebnonnasir A. Production of nanostructured WC–Co powder by ball milling. International Journal of Refractory Metals and Hard Materials. 2009; 27; 159-163.
[12] Fabijanić TA, Alar Z, Ćorić D. Influence of consolidation process and sintering temperature on microstructure and mechanical properties of near nano- and nano-structured WC-Co cemented carbides. International Journal of Refractory Metals and Hard Materials. 2016; 54; 82-89.

[13] Emani SV, Wang C, Shaw LL, Chen Z. On the hardness of submicrometer-sized WC–Co materials. Materials Science and Engineering: A. 2015; 628; 98–103.
[14] Ferreira JAM, Amaral MAP, Antunes FV, Costa JDM. A study on the mechanical behaviour of WC/Co hardmetals. International Journal of Refractory Metals and Hard Materials. 2009; 27; 1-8.
[15] Wang D, Liu W, Feng Q, Dong C, Liu Q, Duan L, et al. Effect of inorganic/organic ratio and chemical coupling on the performance of porous silica/chitosan hybrid scaffolds. Materials Science and Engineering: C. 2017; 70; 969–975.
[16] Lawley A, Murphy TF. Metallography of powder metallurgy materials, Materials Characterization. 2003; 51; 315-327.
[17] ASTM E384: Standard Test Method for Microindentantion Hardness of Materials. ASTM. 2009; 1–8.
[18] Cullity BD, Stock SR. Elements of X-Ray Diffraction. 3nd. ed. Pearson Education Limited. 2014.
[19] Larson AC, Von Dreele RB. General Structure Analysis System (GSAS). Los Alamos National Laboratory Report LAUR. 2000.
[20] Bish DL, Chipera SJ. Problems and solutions in quantitative analysis of complex mixtures by X-ray powder diffraction. Advances in X-ray Analysis. 1987; 31; 295-308.
[21] Homepage BDEC - Bases of crystalline structures [homepage on the internet]. Brazil: BDEC, 2018 [cited 2018 Mar 21]. Available from: http://bdec.dotlib.com.br/
[22] O'Connor BH, Raven MD. Application of the Rietveld refinement procedure in assaying powdered mixtures. Powder Diffraction; 1988; 3; 2–6.
[23] Yongtao Z, Haibo H, Lede M, Hanqian Z, Jinfu L. Quantitative carbide analysis using the Rietveld method for 2.25Cr–1Mo–0.25V steel. Materials Characterization; 2009; 60; 953-956.
[24] Khalili S, Soleimanian V, Mokhtari A. Developing a method for the evaluation of dislocation parameters from the Rietveld refinement procedure. Powder Diffraction. 2016; 31(3); 198-204.
[25] Manfridini APA, Godoy GCD, Santos LA. Structural characterization of plasma nitrided interstitial-free steel at different temperatures by SEM, XRD and Rietveld method. Journal of Materials Research and Technology. 2017; 6; 65-70.
[26] Rocha AC, Nascimento AV, Margarit M, Pereira IC, Santos AK, OR Mattos. Abrasive blasting contamination in Super Duplex and carbon steels - a quantification approach by Rietveld analysis. Materials Research. 2014; 17; 1356-1366.
[27] Pala Z, Fojtikova J, Koubsky T, Musalek R, Strasky J, Capek J, Kolarik K. Study of residual stresses, microstructure, and hardness in FeB and Fe2B ultra-hard layers. Powder Diffraction. 2015; 30(1); 83-89.
[28] Tolédano P, Krexner G, Prem M, Weber HP, Dmitriev VP. Theory of the martensitic transformation in cobalto. Physical Review B. 2001; 64; 144104.
[29] Das A, Chakraborti PC, Tarafder S, Bhadeshia HKDH. Analysis of deformation induced martensitic transformation in stainless steels. Materials Science and Technology. 2011; 27(1); 366-370.
[30] Raihanuzzaman RM, Jeong TS, Ghomashchi R, Xie Z, Hong SJ, Characterization of short-duration high-energy ball milled WC–Co powders and subsequent consolidations. Journal of Alloys and Compounds. 2014; 615(1); 564-568.
[31] Oliver CJRG, Álvarez EA, García JL. Kinetics of densification and grain growth in ultrafine WC-Co composites. International Journal of Refractory Metals and Hard Materials. 2016; 59; 121-131.
[32] Guillermet AF. Thermodynamic Properties of the Co-W-C system. Metallurgical Transactions A. 1989; 20; 935.
[33] Suetin DV, Shein IR, Ivanovskii AL. Structural, electronic and magnetic properties of η carbides (Fe3W3C, Fe6W6C, Co3W3C and Co6W6C) from first principles calculations. Physica B: Condensed Matter. 2009; 404; 3544-3549.
[34] Morelhão SL. Computer Simulation Tools for X-ray Analysis - Scattering and Diffraction Methods. 1 nd. ed. Springer International Publishing; 2016.
[35] Ponomarev SS, Shatov AV, Mikhailov AA, Firstov SA. Carbon distribution in WC based cemented carbides. International Journal of Refractory Metals and Hard Materials. 2015; 49; 42-56.
[36] Emani SV, Santos AFRC, Shaw LL, Chen Z. Investigation of microstructure and mechanical properties at low and high temperatures of WC–6wt% Co. International Journal of Refractory Metals and Hard Materials. 2016; 58; 172-181.
[37] Lin H, Sun J, Li C, He H, Qin L, Li Q. A facile route to synthesize WC–Co nanocomposite powders and properties of sintered bulk. Journal of Alloys and Compounds. 2016; 682; 531-536.
[38] Kurlov AS, Rempel' A A. Effect of sintering temperature on the phase composition and microhardness of WC-8wt% Co cemented carbide. Journal Inorganic Materials. 2007; 43(6); 602-607.
[39] Pötschke J, Säuberlich T, Vornberger A, Meese-Marktscheffel JA. Solid state sintered nanoscaled hardmetals and their properties. International Journal of Refractory Metals and Hard Materials. 2018; 72; 45-50.
[40] Fabijanić TA, Alar Z, Pötschke J. Potentials of nanostructured WC–Co hardmetal as reference material for Vickers hardness. International Journal of Refractory Metals and Hard Materials. 2015; 50; 126-132.
[41] Raihanuzzaman RM, Han ST, Ghomashchi R, Kim HS, Hong SJ. Conventional sintering of WC with nano-sized Co binder: Characterization and mechanical behavior. International Journal of Refractory Metals and Hard Materials. 2015; 53; 2-6.
[42] Zafar S, Sharma AK. Microstructure and wear performance of heat treated WC-12Co microwave clad. Vacuum. 2016; 131; 213-222.
[43] Zafar S, Sharma AK. Structure-property correlations in nanostructured WC–12Co microwave clad. Applied Surface Science. 2016; 370; 92-101.
[44] Yuan Y, Fu L, Li J. Annealing effect on the mechanical properties of ultrafine WC–Co materials. Journal of Applied Research and Technology. 2017; 15; 396-401.
[45] Ahmed R, Faisal NH, Mamour S, et al. 2nd International Multidisciplinary Microscopy and Microanalysis Congress. Springer Proceedings in Physics; 2015. Chapter Microstructural Evaluation of Suspension Thermally Sprayed WC-Co Nanocomposite Coatings, 164, p. 31-38.
[46] Favre TMSJ, Koizumi Y, Chiba A, Fabregue D, Maire E. 3rd International Symposium on High-Temperature Metallurgical Processing. 1nd. ed. The Minerals, Metals, & Materials Society, 2012. Chapter Part IV: Alloy and Materials Preparation, Recrystallization of L-605 cobalt superalloy during hot-working process, p. 257-264.
[47] Lining G, Huang J, Xie C, Effects of carbon content on microstructure and properties of WC–20Co cemented carbides. International Journal of Refractory Metals and Hard Materials. 2014; 42; 228–232.